CHEMISTRY
A EUROPEAN JOURNAL

DOI: 10.1002/chem.200601093

Gas-Phase Chemistry of Diphosphate Anions as a Tool To Investigate the Intrinsic Requirements of Phosphate Ester Enzymatic Reactions: The $[M^1M^2HP_2O_7]^-$ Ions

Federico Pepi,[a] Vincenzo Barone,[b] Paola Cimino,[b, c] and Andreina Ricci*[a]

Abstract: Experimental studies on gaseous inorganic phosphate ions are practically nonexistent, yet they can prove helpful for a better understanding of the mechanisms of phosphate ester enzymatic processes. The present contribution extends our previous investigations on the gas-phase ion chemistry of diphosphate species to the $[M^1M^2HP_2O_7]^-$ ions where M^1 and M^2 are the same or different and correspond to the Li, Na, K, Cs, and Rb cations. The diphosphate ions are formed by electrospray ionization of 10^{-4} M solutions of $Na_5P_3O_{10}$ in CH_3CN/H_2O (1/1) and MOH bases or M salts as a source of M^+ cations. The joint application of mass spectrometric techniques and quantum-mechanical calculations makes it possible to characterize the gaseous $[M^1M^2HP_2O_7]^-$ ions as a mixed ionic population formed by two isomeric species: linear diphosphate anion coordinated to two M^+ cations (group **I**) and $[PO_3\cdots M^1M^2\cdots HPO_4]^-$ clusters (group **II**). The relative gas-phase stabilities and activation barriers for the isomerization **I**→**II**, which depend on the nature of the M^+ cations, highlight the electronic susceptibility of P-O-P bond breaking in the active site of enzymes. The previously unexplored gas-phase reactivity of $[M^1M^2HP_2O_7]^-$ ions towards alcohols of different acidity was investigated by Fourier transform ion cyclotron resonance mass spectrometry (FT-ICR/MS). The reaction proceeds by addition of the alcohol molecule followed by elimination of a water molecule.

Keywords: ab initio calculations · alkali metals · anions · gas-phase reactions · mass spectrometry

Introduction

The reactions of phosphate esters and anhydrides are of fundamental importance in the living world and play a crucial role in numerous basic cellular functions.[1] These species are extremely inert under laboratory conditions, but under enzymatic conditions the rate enhancements of their reactions are among the largest established to date.[2] The proficiency of enzymes catalyzing phosphate ester processes have constantly encouraged a huge number of experimental[3–8] and theoretical[9–15] studies aimed at explaining how this catalysis is achieved. However, despite the great deal of information obtained, there are still unresolved issues. Two limiting scenarios can be used to describe the variety of mechanisms of phosphoryl transfer reactions: the dissociative and associative pathways, which refer to the distances between the phosphate moiety, the nucleophile and the leaving group in the transition state. In the dissociative mechanism ($D_n + A_n$), the bond between phosphorus and the leaving group has largely broken before approach of the nucleophile and the reaction proceeds via a metaphosphate-like transition state [Eq. (1)]. Conversely, if the incoming nucleophile

$$R^1OPO_3H^- \longrightarrow R^1OH + PO_3^- \xrightarrow{R^2OH} R^2OPO_3H^- \quad (1)$$

bonds to the phosphate group before the leaving group departs, a pentavalent phosphorus intermediate (phosphorane) is formed, and the reaction is said to proceed via the associative mechanism (A_n+D_n) [Eq. (2)].

[a] Prof. F. Pepi, Prof. A. Ricci
Dip.to di Studi di Chimica e Tecnologia delle Sostanze Biologicamente Attive
Università degli Studi di Roma "La Sapienza"
P.le A. Moro, 5, 00185, Rome (Italy)
Fax: (+39) 064-991-3602
E-mail: andreina.ricci@uniroma1.it

[b] Prof. V. Barone, Dr. P. Cimino
Dip.to di Chimica, Università degli Studi di Napoli "Federico II"
M.te S. Angelo, Via Cinzia, 80100, Naples (Italy)

[c] Dr. P. Cimino
Permanent address:
Dip.to di Scienze Farmaceutiche, Università di Salerno
via Ponte don Melillo, 84084, Fisciano (SA) (Italy)

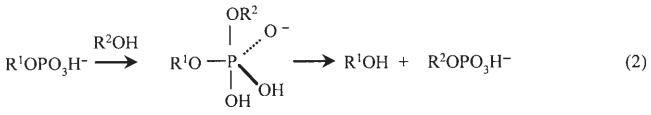

(2)

The more important prerequisites for efficient enzymatic cleavage of phosphate esters include: the presence of a nucleophilic group to which the phosphoryl group is transferred, a basic moiety to activate and correctly arrange the nucleophile, a general acid to protonate the leaving group, and one or more positively charged groups to stabilize the phosphoanion transition state. In the active enzymatic site these requirements are satisfied by coordination with different amino acid groups and, in many enzymes, by using metal cations as cofactors.[16–19] In enzymatic hydrolysis reactions metal cations play a key catalytic role by lowering the pK_a of a directly coordinated water molecule and by allowing the resulting hydroxyl ions to act as nucleophile or general base. Alternatively, the water molecule coordinated to the metal ion can efficiently protonate the leaving group. Furthermore, metal cations stabilize the negative charges of the transition states. The role of metal cations, besides the specific interest in the mechanistic aspects of enzyme action, has been extensively investigated in studies on biomimetic catalysis of phosphate esters.[20–22]

In gaseous media the impact of environmental factors is dramatically reduced, and gas-phase studies can offer the possibility of investigating the intrinsic requirements of enzymatic processes. Despite this, experimental gas-phase studies on anionic inorganic polyphosphate species and their reactions are relatively scant. To the best of our knowledge, the only experimental information available on anionic inorganic phosphate species in the gas phase is related to the thermodynamic and kinetic properties of metaphosphate anion, PO_3^-,[23a] the hydration free energies of singly and doubly charged phosphate and diphosphate anions,[23b] the electron-detachment energies of $H_2PO_4^-$, $H_2P_2O_7^{2-}$, and $H_3P_3O_{10}^{2-}$,[24] and the quali- and quantitative analysis of inorganic polyphosphates[25] by mass spectrometric techniques. Generation of polyphosphate from sodiated clusters of phosphate ions has been hypothesized under conditions of collisionally activated mass spectrometry.[26] Other studies have focussed on the reaction of phosphate ion and its $[H_3PO_4\cdots H_2PO_4]^-$ cluster with trimethylborate,[27] and the estimation of the relative activation barrier for decay by electron detachment or ionic fragmentation of triphosphate dianions in a quadrupole ion trap.[28] Finally, gas-phase alkylation of triphosphate and DNA anions by alkylammonium cations in molecular clusters has been reported.[29]

Most theoretical work is related to the mechanism of phosphate ester hydrolysis, and little attention has been devoted to the inorganic phosphoanhydride compounds despite their importance in biological systems. The simplest compound containing the P-O-P moiety, $H_4P_2O_7$, diphosphoric acid, has been the subject of computational investigations focussed on its gas-phase structure, as well as those of its ions and complexes with singly and doubly charged metal ions. These studies provided insights into the thermochemistry of the hydrolysis reaction and into the role played by the metal cation and by solvation.[30–33] In particular it has been demonstrated that Mg^{2+} coordination elongates one of the P–O bridging bonds in the $[MgH_nP_2O_7]^{(2-n)-}$ ions ($n=0$, 1, 2), and plays a catalytic role in their isomerization to $[H_nPO_4\cdots Mg\cdots PO_3]^{(2-n)-}$.

As far as phosphate ester reactions are concerned, most studies have focussed on hydrolysis, owing to the bioenergetic importance of this process and its role in nucleic acid biochemistry. Little attention has been devoted to reactions with alcohols and thiols, in spite of the existence of many enzymes utilizing phosphoserine and phosphocysteine amino acid residues to accomplish P-O-P bond cleavage. The only systematic reactivity studies in the gas phase have focussed on the reaction of phosphate and phosphonate esters, such as trimethyl phosphate (TMP) and dimethyl methylphosphonate and its conjugate base $(CH_3O)_2P(O)CH_2^-$ with several anions and neutral substrates, respectively, which were examined by FT-ICR mass spectrometry and the flowing afterglow technique.[34] Self-condensation ion–molecule reactions of organophosphorus esters such as trimethyl phosphate, trimethyl phosphite, triethyl phosphate and dimethyl phosphonate were investigated by ion-trap mass spectrometry and FT-ICR mass spectrometry.[35] The reaction of alcohols and TMP in the gas phase[34a,b] leads to the observation of traces of products arising from alcoholysis at the phosphorus atom. A recent quantum mechanical study on the thiolysis and alcoholysis of phosphate tri- and monoesters with alkyl and aryl leaving groups found that triesters react exclusively via an associative pathway, and monoester phosphates can react by both the associative and dissociative mechanisms, depending on the basicity of the attacking and leaving groups.[36]

No theoretical or experimental studies have been reported on the reactions of gaseous inorganic polyphosphate species with alcohols.

Our systematic investigation on the gas-phase ion chemistry of inorganic polyphosphate species started with the diphosphate anion $H_3P_2O_7^-$,[37] the simplest compound containing the P-O-P moiety, and then went on to consider the effects of the first water molecule of solvation and of alkali metal coordination, by investigating the structure and reactivity of $H_5P_2O_8^-$[38] and $MH_2P_2O_7^-$ ions (M = Li, Na, K, Rb, Cs),[39] respectively. These studies were carried out by the joint application of mass spectrometric techniques [electrospray ionization Fourier transform ion cyclotron resonance MS (ESI-FTICR/MS) and ESI triple-quadrupole MS (ESI-TQ/MS)] and theoretical methods. Endothermic or kinetically hampered reactions of diphosphate species were induced in collisionally activated dissociation (CAD) mass spectrometric experiments, and the mechanisms investigated with theoretical methods. The results obtained in these studies can provide a benchmark for enhanced understanding of the mechanisms and factors controlling phosphate ester reactions in living organisms.

The present contribution extends the picture of the gas-phase chemical behavior of phosphate species by considering the effect of coordination of a second alkali metal cation. The gas-phase structures and reactivity of $[M^1M^2HP_2O_7]^-$ ions, where M^1 and M^2 are the same or different and correspond to the Li, Na, K, Cs, and Rb cations were investigated by using the powerful integrated combination of mass spectrometric (FT-ICR-, TQ-MS) and theoretical calculations at the Kohn–Sham and post-Hartree–Fock levels of theory.

Results

Structural characterization of $M_2HP_2O_7^-$ ions

ESI/TQ CAD mass spectrometric experiments: The ESI mass spectrum of a solution of LiOH and $Na_5P_3O_{10}$ in CH_3CN/H_2O (1/1) shows the $Li_2HP_2O_7^-$, $NaLiHP_2O_7^-$, and $Na_2HP_2O_7^-$ ions (Figure 1a), and that of a solution of

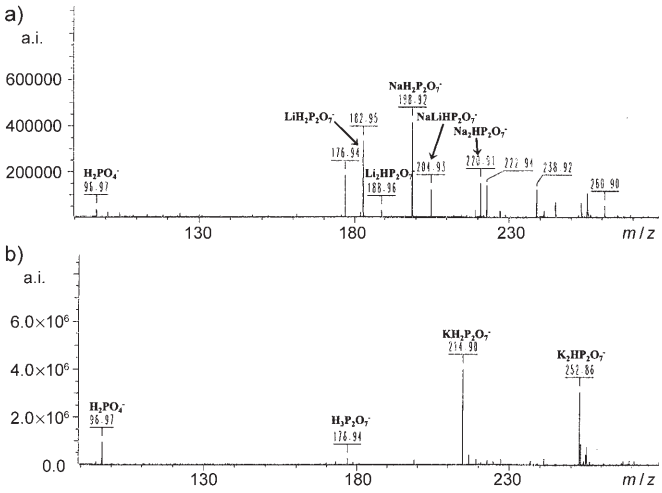

Figure 1. a) ESI spectrum of CH_3CN/H_2O (1/1) solution of $Na_5P_3O_{10}$ and LiOH (1/1). b) ESI spectrum of CH_3CN/H_2O (1/1) solution of $K_4P_2O_7$.

$K_4P_2O_7$ in CH_3CN/H_2O (1/1) (Figure 1b) shows the $K_2HP_2O_7^-$ ion. Very low intensities of the $Rb_2HP_2O_7^-$ and $Cs_2HP_2O_7^-$ ions are observed in the ESI spectra of solutions containing $Na_5P_3O_{10}$ and RbOH or CsOH. The CAD spectra of the $M^1M^2HP_2O_7^-$ ($M^1=M^2=$Li, Na, K) ions display only the PO_3^- fragment at m/z 79 corresponding to the loss of the M_2HPO_4 moiety. The energy-resolved CAD spectra of the $M_2HP_2O_7^-$ ions (Figure 2) show the relative intensity profiles of the fragment at m/z 79. Formation of the PO_3^- fragment is influenced by the nature of the cations involved and occurs at decreasing energy with decreasing charge-to-radius ratio of the metal cation.

Validation of the computational approach: The most suitable level of theory was assessed by computing the energies governing the reactions of the compounds under study at

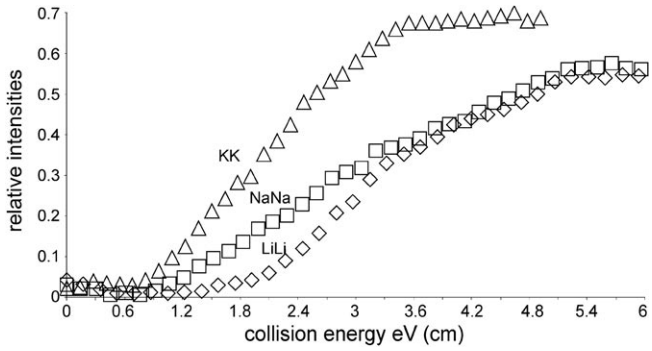

Figure 2. Energy-resolved CAD spectra of the $M_2HP_2O_7^-$ ions showing the profile of the intensities of the fragment at m/z 79 resulting from loss of the M_2HPO_4 molecule.

various levels. To estimate reliable energies in the most effective way we used the following composite formula: $\Delta E_{best} = E_{CCSD(T)/6\text{-}31+G(d)} + [E_{MP2/6\text{-}311+G(2df,2dp)} - E_{MP2/6\text{-}31+G(d)}]$, where the subscripts denote the level of theory. The calculated energies in Table 1 show that the results delivered by hybrid functionals (here B3LYP) can differ from those issuing from MP2 and CCSD(T) computations, but the reactivity trends are always the same. Moreover, basis set extension [6-31+G(d), 6-311+G(2df,2dp)] introduces systematic modifications into the results with negligible effect on general trends (Table 1), and the diffuse functions on non-oxygen atoms have a negligible role.

Thus, to allow direct comparison with the previously reported data,[37–39] we mainly refer in the following to B3LYP/6-31+G(d) results. It is well known that the nonpotential terms can be reliably evaluated at the B3LYP/6-31+G(d) level.[44] In all cases, we evaluated the electronic energy differences ΔE together with the corresponding free energies ΔG, which include zero-point, thermal and entropic contributions. Table 2 shows that ΔE, ΔU, ΔH and ΔG have parallel trends: as a consequence the results are presented in terms of energies, with interpretation based on electronic contributions only.

Quantum-mechanical results: To gain information on the structure of gaseous $M^1M^2HP_2O_7^-$ ions investigated by mass spectrometric techniques we undertook a systematic theoretical study at the B3LYP/6-31+G(d) level of theory. Studying the $M^1M^2HP_2O_7^-$ potential energy surfaces led to the characterization of several structural isomers of the species of interest. They are labeled by a Roman numeral followed by the chemical symbol of the two coordinated metal cations. Group **I** (Figures 3–6) corresponds to the linear $M^1M^2HP_2O_7^-$ ions, in which $HP_2O_7^{3-}$ is coordinated to two M^+ ions. Group **II** (Figure 7) corresponds to a cluster structure in which two M^+ ions hold together the PO_3^- and HPO_4^{2-} anions by electrostatic interactions. For example, the $NaKHP_2O_7^-$ ion is indicated by **I_NaK** or **II_NaK**, and the $Na_2HP_2O_7^-$ ion by **I_2Na** or **II_2Na**. Group **III** (Figure 7) corresponds to the cluster formed by the HPO_4^{2-} ion and two M^+ ions.

Table 1. Energy differences ΔE [kcal mol^{-1}] and activation barriers $\Delta E^{\neq}$ [kcal mol^{-1}] of the processes under investigation for the diphosphate anions under standard conditions (298.15 K, 1 atm) in the gas phase at different levels of theory and with several basis sets.

$Li_2HP_2O_7^-$	ΔE[a]	ΔE[b]	ΔE[c]	ΔE[d]	ΔE[e]	ΔE[f]	ΔE_{best}[g]
Ia	0.0	0.0	0.0	0.0	0.0	0.0	0.0
Ib	10.5	11.5	7.7	7.9	8.8	8.1	9.1
Ic	15.5	16.0	12.1	12.1	12.7	12.6	13.2
IIa	3.3	3.8	3.7	3.8	5.5	4.4	6.1
IIb	10.4	12.8	11.0	11.0	15.5	12.1	16.6
III + PO_3^-	60.0	58.2	64.2	64.1	63.6	66.2	65.7
	$\Delta E^{\neq}$[a]	$\Delta E^{\neq}$[b]	$\Delta E^{\neq}$[c]	$\Delta E^{\neq}$[d]	$\Delta E^{\neq}$[e]	$\Delta E^{\neq}$[f]	$\Delta E^{\neq}_{best}$[g]
Ia→**IIa**	4.9	6.0	–	4.1	6.8	4.4	7.2
Ia→**IIb**	33.2	34.4	–	33.2	33.5	35.3	35.7
$Na_2HP_2O_7^-$	ΔE[a]	ΔE[b]	ΔE[c]	ΔE[d]	ΔE[e]	ΔE[f]	ΔE_{best}[g]
Ia	0.0	0.0	0.0	0.0	0.0	0.0	0.0
Ib	0.2	−1.2	−0.3	−0.1	−1.1	−0.7	−1.6
Ic	1.1	0.6	−1.0	−0.9	−1.4	−0.8	−1.3
Id	4.4	5.0	7.0	7.2	8.4	7.1	8.3
IIa	1.8	1.4	6.2	6.4	7.9	7.0	8.5
IIb	9.3	10.7	13.9	14.2	18.0	15.3	19.1
III + PO_3^-	51.0	49.9	56.9	57.0	56.7	58.4	58.1
	$\Delta E^{\neq}$[a]	$\Delta E^{\neq}$[b]	$\Delta E^{\neq}$[c]	$\Delta E^{\neq}$[d]	$\Delta E^{\neq}$[e]	$\Delta E^{\neq}$[f]	$\Delta E^{\neq}_{best}$[g]
Ia→**Id**	6.6	6.6	–	8.5	9.2	8.4	9.1
Ia→**IIa**	0.5	0.7	–	0.7	1.7	0.8	1.9
Ia→**IIb**	29.0	30.0	–	28.9	28.9	31.3	31.2
$K_2HP_2O_7^-$	ΔE[a]	ΔE[b]	ΔE[c]	ΔE[d]	ΔE[e]	ΔE[f]	ΔE_{best}[g]
Ia	0.0	0.0	0.0	0.0	0.0	0.0	0.0
Ib	2.0	1.4	4.9	4.7	3.4	3.5	2.2
Ic	4.1	3.0	5.9	5.9	5.1	5.6	4.8
IIa	9.5	9.4	18.0	17.9	17.4	17.1	16.7
IIb	17.8	19.3	26.0	25.8	27.6	25.9	27.7
III + PO_3^-	47.8	46.4	59.7	59.6	57.0	54.7	52.1
	$\Delta E^{\neq}$[a]	$\Delta E^{\neq}$[b]	$\Delta E^{\neq}$[c]	$\Delta E^{\neq}$[d]	$\Delta E^{\neq}$[e]	$\Delta E^{\neq}$[f]	ΔE_{best}[g]
Ia→**Ic**	11.4	10.6	–	13.6	13.1	12.9	12.4
Ic→**IIa**	9.9	10.8	–	13.2	13.3	12.6	12.6
Ic→**IIb**	30.5	32.5	–	30.8	31.2	32.7	33.1

[a] opt B3LYP/6-31+G(d). [b] sp B3LYP/6–311+G(2df,2pd). [c] opt MP2/6-31+G(d). [d] sp MP2/6-31+G(d). [e] sp MP2/6–311+G(2df,2pd). [f] sp CCSD(T)/6-31+G(d) diffuse on oxygen. [g] ΔE_{best} and $\Delta E^{\neq}_{best}$: CCSD(T)/6-31+G(d)+[MP2/6-311+G(2df,2pd)−MP2/6-31+G(d)].

Finally, for each group of isomers **I**, **II** and **III**, the letter **a** indicates the most stable structure, and the letters **b**, **c** and so on refer to different isomers of decreasing stability. We restrict our theoretical analysis to $M^1M^2HP_2O_7^-$ with $M^1 = M^2 = Li$, Na, K and, for the purpose of structural comparison, to the group **I** ions with $M^1 = Li$ and $M^2 = Na$.

Tables 1 and 2 report the relative stabilities and dissociation energies of the different $M_2HP_2O_7^-$ ions and the energy barriers for the isomerization processes computed at the B3LYP/6-31+G(d) level of theory. The most significant isomerization processes are schematically shown in Figures 8–10. Transition-state structures involved in the isomerization processes are shown in Figure 11.

The $[M^1M^2HP_2O_7]^-$ ions (group I): Figures 3–6 show the optimized geometries at the B3LYP/6-31+G(d) level of theory of the ions formed by the linear $HP_2O_7^{3-}$ ion and two M^+ ions held together by electrostatic interactions (group **I**). In the $[M^1M^2HP_2O_7]^-$ ions, the cations M^1 and M^2 are preferentially bonded to two oxygen atoms of different phosphate groups, rather than to the oxygen atoms of the same phosphate group. Two of the negative charges are localized on the same phosphate group and the excess negative charge residing on the oxygen atoms of the phosphate moiety not binding the OH group makes the corresponding P–O bridging bond longer. The equilibrium structure of the most stable $Li_2HP_2O_7^-$ isomer (Figure 3, Figure 8), the **I_2Li_a** ion, is 10.5 and 15.5 kcal mol^{-1} lower in energy than **I_2Li_b** and **I_2Li_c**, respectively. The last two structures exhibit an H-bond between the proton and one of the oxygen atoms of the adjacent phosphate group. In the **I_2Li_a** ion, the P1–O2 and P6–O2 bond lengths are 1.602 and 1.816 Å, respectively, and the P-O-P angle is 128.5°.

The potential energy surface of the **I_LiNa** ions shows two more stable, almost isoenergetic, structures (Figure 6), both characterized by the absence of the internal hydrogen bond. Our computations indicate that the **I_LiNa_a** isomer is 0.7 kcal mol^{-1} more stable than **I_LiNa_c** and 4.3 kcal mol^{-1} more stable than **I_LiNa_b**. The geometry of **I_LiNa_c** is nevertheless characterized by the presence of

Table 2. Energy differences and activation barriers in kcal mol^{-1} of the processes under investigation for the diphosphate anions with (ΔE_0 and ΔE_0^{+}) and without (ΔE and ΔE^{+}) zero-point contributions and activation parameters under standard conditions (298.15 K, 1 atm): internal energy (ΔU and ΔU^{+}), enthalpy (ΔH and ΔH^{+}) and free energy (ΔG and ΔG^{+}) in the gas phase (B3LYP/6-31+G*).

$Li_2HP_2O_7^-$	ΔE	ΔE_0	ΔU	ΔH	ΔG
Ia	0.0	0.0	0.0	0.0	0.0
Ib	10.5	10.8	10.5	10.5	11.3
Ic	15.5	14.9	14.2	14.2	16.0
IIa	3.3	2.6	3.0	3.0	1.8
IIb	10.4	9.6	10.0	10.0	8.6
III+PO_3^-	60.0	58.1	57.7	58.3	46.2
	ΔE^{+}	ΔE_0^{+}	ΔU^{+}	ΔH^{+}	ΔG^{+}
Ia→**IIa**	4.9	4.2	4.0	4.0	4.7
Ia→**IIb**	33.2	33.2	30.0	30.0	30.4
$Na_2HP_2O_7^-$	ΔE	ΔE_0	ΔU	ΔH	ΔG
Ia	0.0	0.0	0.0	0.0	0.0
Ib	0.2	0.0	0.4	0.4	−0.3
Ic	1.1	1.3	1.4	1.4	1.1
Id	4.4	3.9	4.6	4.6	2.0
IIa	1.8	0.8	1.9	1.9	−1.4
IIb	9.3	8.3	9.3	9.3	5.8
III+PO_3^-	51.0	49.1	49.2	49.8	36.1
	ΔE^{+}	ΔE_0^{+}	ΔU^{+}	ΔH^{+}	ΔG^{+}
Ia→**Id**	6.6	6.0	6.1	6.1	6.0
Ic→**Ib**	9.5	9.2	8.9	8.9	9.9
Id→**Ib**	0.1	0.2	−0.4	−0.4	1.8
Ic→**Ia**	−0.3	−0.5	−0.6	−0.6	−1.2
Ia→**IIa**	0.5	0.3	−0.2	−0.2	1.6
Ia→**IIb**	29.0	26.5	26.0	26.1	27.6
$K_2HP_2O_7^-$	ΔE	ΔE_0	ΔU	ΔH	ΔG
Ia	0.0	0.0	0.0	0.0	0.0
Ib	2.0	1.6	1.1	1.1	1.9
Ic	4.1	3.6	4.0	4.0	3.2
IIa	9.5	7.8	9.2	9.2	4.3
IIb	17.8	16.1	16.8	16.8	13.6
III+PO_3^-	47.8	45.6	45.8	46.4	31.7
	ΔE^{+}	ΔE_0^{+}	ΔU^{+}	ΔH^{+}	ΔG^{+}
Ia→**Ic**	11.4	10.2	10.3	10.3	9.6
Ic→**IIa**	9.9	8.7	9.0	9.0	7.4
Ic→**IIb**	30.5	27.6	27.4	27.4	27.3

the H-bond. In the **I_LiNa_a** ion, the P1−O2 and P6−O2 bond lengths are 1.606 and 1.862 Å, respectively, and the P-O-P angle is 136.4°. The P6−O2 distance is about 0.046 Å longer than in the **I_2Li_a** ion, and this suggests the effect of the reduced screening of the negative charge on phosphorus electron density and the P-O-P bond length.

Except for $M^1=M^2=$Li and for $M^1=$Li, $M^2=$Na, an H-bond is present in all the most stable structures of the $[M^1M^2HP_2O_7]^-$ ions.

In the **I_2Na_a** ion (Figure 4) all five hydrogen-free phosphate oxygen atoms are coordinated, four to the metal cations and one to the hydrogen atom of the adjacent OH group. The P-O-P bond angle is 134.6° and the P1−O2 and P6−O2 bond lengths are 1.655 and 1.787 Å, respectively.

Furthermore, our computations suggest that the **I_2Na_a** and **I_2Na_b** isomers are nearly isoenergetic and more stable than **I_2Na_c** and **I_2Na_d** by 1.1 and 4.4 kcal mol^{-1}, respectively.

Both **I_2Na_b** and **I_2Na_d** do not exhibit an H-bond. In **I_2Na_b** the oxygen atoms are in the staggered conformation and both Na^+ ions are coordinated by two O atoms of P1 and one O atom of P6 atom. The P6−O2 distance of 1.777 Å and the P-O-P bond angle of 134.6° do not differ appreciably from those of **I_2Na_a**. In the less stable **I_2Na_d**, the oxygen atoms are in the eclipsed configuration, the P6−O2 bond is 1.954 Å long and the P-O-P bond angle becomes as large as 150°. The P6−O2 distance is 0.14 Å longer than in the **I_2Li_a** ion and about 0.10 Å longer than in the **I_LiNa_a** ion.

The isomerization of **I_2Na_a** to **I_2Na_d**, corresponding to breaking of the hydrogen bond, is endothermic by 4.4 kcal mol^{-1} and has an activation barrier of 6.6 kcal mol^{-1} (Figure 9).

For the **I_2K** ions (Figure 5) we found two different stable structures both characterized by the presence of the internal hydrogen bond (the **I_2K_a** and **I_2K_b** isomers) with a computed energy difference of 2.0 kcal mol^{-1} (Figure 10). In the **I_2K_a** structure, the P-O-P angle of 129.5° and the P1−O2 and P6−O2 distances of 1.655 and 1.785 Å, respectively, are very similar to those in the **I_2Na_a** ion. Comparison of the **I_2K_a** geometries with those of the **I_2K_b** and **I_2Na_a** ions clearly shows that the electrostatic repulsions are partially offset by staggering the oxygen atoms. In the **I_2K_b** ions, which show an eclipsed configuration, the P-O-P angle is 134.8° and the P1−O2 and P6−O2 bond lengths are 1.660 and 1.799 Å, respectively.

The $[HPO_4\cdots M^1,M^2\cdots PO_3]^-$ clusters (group II): Figure 7 shows the optimized structures for all the group **II** ions formed by HPO_4^{2-} and PO_3^- held together by two M^+ cations. In the most stable $[HPO_4\cdots M^1,M^2\cdots PO_3]^-$ clusters, labeled **II_a**, the metal cations are coordinated to the metaphosphate group through two oxygen atoms and to the hydrogenphosphate ion through all three proton-free oxygen atoms.

The metal cations are coordinated to the hydrogenphosphate ion through two proton-free oxygen atoms and by the OH group in isomer **II_b**. The main differences arising from the change in metal coordination are found in the M−O distances, which increase with decreasing charge-to-radius ratios.

As reported in Table 1 the dissociation energy of clusters **II_a** into the PO_3^- ion and the M_2HPO_4 moiety depends on the nature of the metal cations involved. This process is computed to be endothermic by 56.7 kcal mol^{-1} for $M^1=M^2=$Li, 49.2 kcal mol^{-1} for $M^1=M^2=$Na and 38.3 kcal mol^{-1} for $M^1=M^2=$K.

The isomerization of the $[M^1M^2HP_2O_7]^-$ ions **I_a** to the $[HPO_4\cdots M^1,M^2\cdots PO_3]^-$ ions **II_a**, the energy profile of which is illustrated in Figures 8–10, is an important pathway, since the reactions involving phosphate anions resulting in hydrolysis or transfer of the phosphoryl group can occur by a dissociative mechanism (Figure 11).

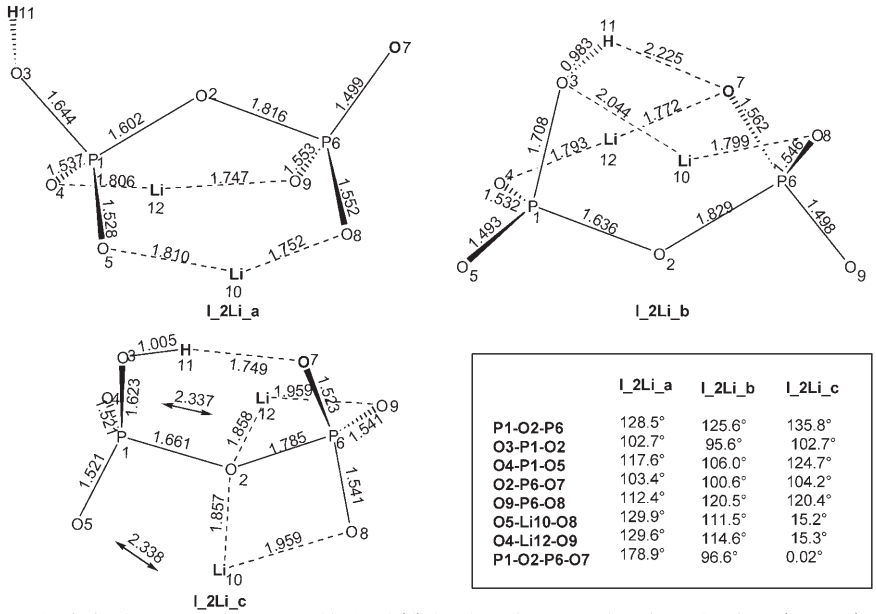

	I_2Li_a	I_2Li_b	I_2Li_c
P1-O2-P6	128.5°	125.6°	135.8°
O3-P1-O2	102.7°	95.6°	102.7°
O4-P1-O5	117.6°	106.0°	124.7°
O2-P6-O7	103.4°	100.6°	104.2°
O9-P6-O8	112.4°	120.5°	120.4°
O5-Li10-O8	129.9°	111.5°	15.2°
O4-Li12-O9	129.6°	114.6°	15.3°
P1-O2-P6-O7	178.9°	96.6°	0.02°

Figure 3. Optimized structures at B3LYP/6-31+G(d) level of theory of the $Li_2HP_2O_7^-$ ions (group **I**). Bond lengths are in angstroms and angles in degrees.

The computed barriers for the **I_2Li_a**→**II_2Li_a**, **I_2Na_d**→**II_2Na_a** and **I_2K_c**→**II_2K_a** isomerizations are 4.9, 0.5, and 9.9 kcal mol^{-1} respectively (Table 2). The whole **I_a**→**II_a** isomerization is endothermic by 3.3, 1.8, and 9.5 kcal mol^{-1} for $M^1=M^2=Li^+$, $M^1=M^2=Na^+$ and $M^1=M^2=K^+$, respectively, at the B3LYP/6-31+G(d) level of theory.

At least in principle, the **I**→**II** isomerization could proceed also by a different mechanism involving proton shift to the bridging oxygen atom (Figure 11). This process was assumed to be responsible for the formation of the PO_3^- fragment ion in the CAD spectra of the $H_3P_2O_7^-$ and $MH_2P_2O_7^-$ ions. For the $M_2HP_2O_7^-$ ions, the activation barriers of 33.2, 29.0 and 30.5 kcal mol^{-1} for $M^1=M^2=Li^+$, $M^1=M^2=Na^+$ and $M^1=M^2=K^+$ respectively (Figures 8–10), indicate that this process is strongly unfavorable with respect to the isomerization involving direct P-O-P bond breaking.

The characterization of the transition-state (TS) structures (Figure 11) established that isomerization preferentially occurs with direct cleavage of the O2–P6 bond in the group **I** ions, characterized by the absence of the intramolecular H-bond, as opposed to proton transfer to O2 with cleavage of the same bond. Indeed, the former reaction is governed by a lower free-energy barrier than the latter.

The [HPO_4···M^1,M^2] clusters (group III): Figure 7 shows the optimized structures at the B3LYP/6-31+G(d) level of theory for the most stable group **III** clusters formed by the HPO_4^{2-} ion and two M^+ cations (**III_a**). The two metal cations are coordinated to the hydrogenphosphate group through all three proton-free oxygen atoms. Also in this case, the main difference arising from the change in metal

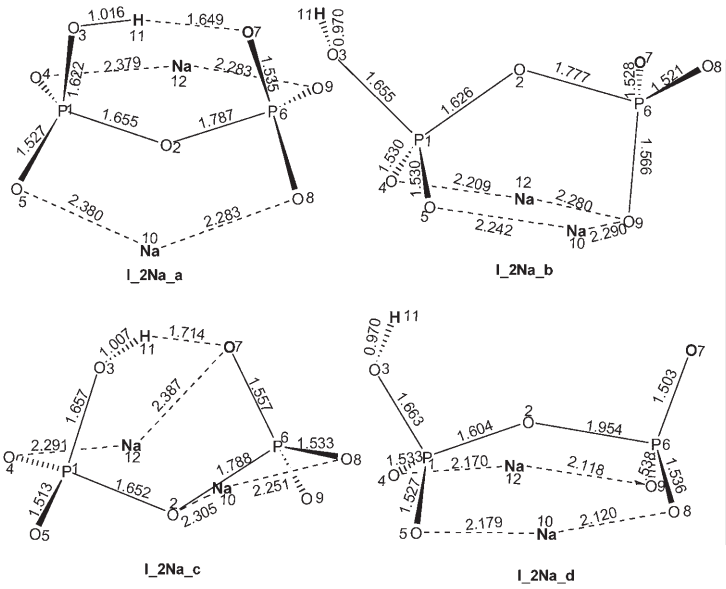

	I_2Na_a	I_2Na_b
P1-O2-P6	134.6°	128.0°
O3-P1-O2	103.2°	101.2°
O4-P1-O5	122.2°	120.8°
O2-P6-O7	102.5°	103.8°
O9-P6-O8	119.2°	112.4°
O5-Na10-O8	131.4°	93.4
O4-Na12-O9	131.4°	93.1°
P1-O2-P6-O7	-0.03°	99.4°

	I_2Na_c	I_2Na_d
P1-O2-P6	127.4°	150.0°
O3-P1-O2	100.2°	101.7°
O4-P1-O5	124.8°	118.9°
O2-P6-O7	100.0°	33.9°
O9-P6-O8	122.2°	114.9°
O5-Na10-O8	47.0°	128.0°
O4-Na12-O9	93.9°	127.8°
P1-O2-P6-O7	-16.9°	174.7°

Figure 4. Optimized structures at B3LYP/6-31+G(d) level of theory of the $Na_2HP_2O_7^-$ ions (group **I**). Bond lengths are in angstroms and angles in degrees.

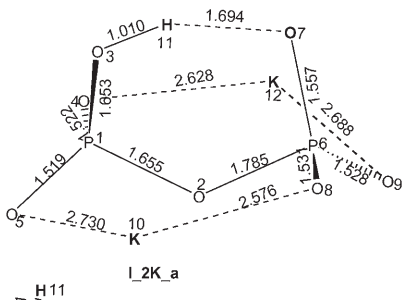

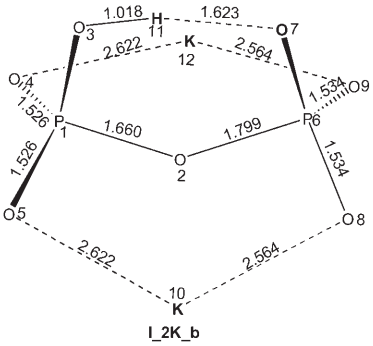

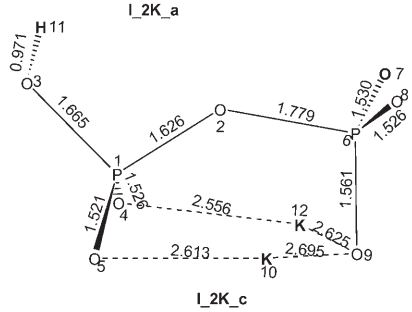

	I_2K_a	I_2K_b	I_2K_c
P1-O2-P6	129.5°	134.8°	132.7°
O3-P1-O2	100.7°	102.5°	99.8°
O4-P1-O5	122.2°	119.7°	120.2°
O2-P6-O7	100.0°	101.6°	104.4°
O9-P6-O8	100.3°	117.5°	113.3°
O5-K10-O8	113.7°	115.1°	83.2°
O4-K12-O9	54.0°	115.1°	83.6°
P1-O2-P6-O7	-16.9°	-0.06°	96.0°

Figure 5. Optimized structures at B3LYP/6-31+G(d) level of theory of the $K_2HP_2O_7^-$ ions (group **I**). Bond lengths are in angstroms and angles in degrees.

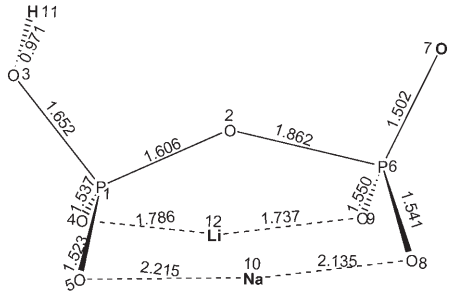

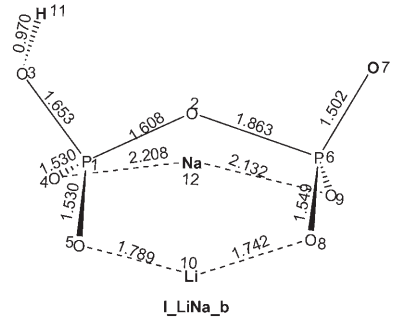

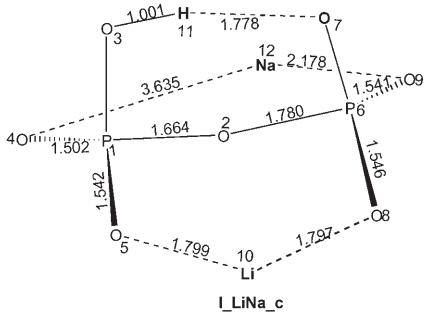

	I_LiNa_a	I_LiNa_b	I_LiNa_c
P1-O2-P6	136.4°	136.5°	126.9°
O3-P1-O2	102.4°	102.1°	101.2°
O4-P1-O5	118.7°	118.1°	120.4°
O2-P6-O7	102.0°	102.0°	103.2°
O9-P6-O8	113.4°	113.4°	116.2°
O5-Na10-O8	122.2°	130.5°	134.5°
O4-Li12-O7	130.0°	123.7°	71.0°

Figure 6. Optimized structures at B3LYP/6-31+G(d) level of theory of the $LiNaHP_2O_7^-$ ions (group **I**). Bond lengths are in angstroms and angles in degrees.

coordination lies in the M–O distances, which increase with decreasing charge-to-radius ratio of the metal cation.

Gas-phase reactivity of $[M^1M^2HP_2O_7]^-$ ions

The $[M^1M^2HP_2O_7]^-$ ions were isolated and thermalized in the FT-ICR cell by collisions with Ar introduced by a pulse valve and then allowed to react with alcohols of different acidity. The main reactivity observed is the addition of an alcohol molecule followed by the elimination of H_2O. A time profile of the ion intensities for the reaction of $Na_2HP_2O_7^-$ with CH_3OH is reported in Figure 12.

Scheme 1 shows a possible pathway for the reaction of $M^1M^2HP_2O_7^-$ ions with alcohols. The ionic product **1**, formally corresponding to addition of the alcohol molecule to the $M^1M^2HP_2O_7^-$ ions, is sometimes observed at longer reaction times, likely when collisional stabilization occurs. The elimination of a water molecule leads to formation of ion **2**, and the addition of a second alcohol molecule to ion **3**. To obtain information on the reaction mechanism we performed two kinds of experiments. First, to evaluate the occurrence of a preliminary and kinetically significant proton-transfer step from the alcohol molecule to the phosphate ion, the $Na_2HP_2O_7^-$ ions were allowed to react with alcohols of different gas-phase acidity. Table 3 reports the rate constants, measured reaction efficiencies (RE) and gas-phase acidities of the alcohols used. Higher rate constants are measured when the $Na_2HP_2O_7^-$ ions are allowed to react with more acidic alcohols. Unit reaction efficiency is obtained with CF_3CH_2OH and $(CF_3)_2CHOH$. When CF_3CH_2OD or CF_3CD_2OD is used, ion **1** loses an HOD molecule.

To investigate the effect of the nature of the metal cation, we studied the reactivity of $M^1M^2HP_2O_7^-$ ions toward the same alcohol. As reported in Table 4, the rate constants measured for the reactions with methanol increase on going from $Li_2HP_2O_7^-$ to $Na_2HP_2O_7^-$. The following reactivity order is observed: $LiNaHP_2O_7^- > Na_2HP_2O_7 > NaKHP_2O_7^- \approx Li_2HP_2O_6^- > K_2HP_2O_7^-$

The $K_2HP_2O_7^-$ and $CsNaHP_2O_7^-$ ions do not react with methanol, and only traces of ionic products are observed with $RbNaHP_2O_7^-$. By comparing the reactivity of $Li_2HP_2O_6^-$, $LiNaHP_2O_7^-$ and $Na_2HP_2O_7^-$ ions towards methanol at the same pressure it seems that the presence of at least one Li^+ ion is of fundamental importance for detecting

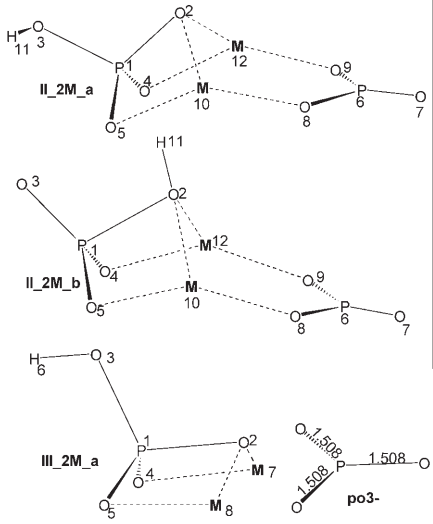

	II_2Li_a	II_2Na_a	II_2K_a	II_2Li_b	II_2Na_b	II_2K_b
P1-O3	1.660	1.875	1.888	1.503	1.512	1.518
P1-O2	1.579	1.575	1.569	1.857	1.867	1.859
P1-O4	1.547	1.550	1.550	1.545	1.543	1.541
P1-O5	1.547	1.550	1.550	1.545	1.543	1.541
O4-M12	1.925	2.243	2.602	1.825	2.161	2.506
O5-M10	1.933	2.225	2.582	1.825	2.161	2.506
O2-M10	1.921	2.248	2.594	2.002	2.298	2.675
O2-M12	1.925	2.247	2.592	2.002	2.298	2.675
O8-M10	1.889	2.236	2.652	1.882	2.230	2.641
O9-M12	1.893	2.242	2.659	1.882	2.229	2.641
P6-O8	1.512	1.511	1.511	1.512	1.511	1.511
P6-O9	1.512	1.511	1.511	1.512	1.511	1.511
P6-O7	1.490	1.492	1.495	1.488	1.491	1.494
P1-O2-P6	18.6°	16.2°	14.1°	20.6°	17.7°	15.8°
O3-P1-O2	110.6°	108.5°	106.5°	104.7°	101.9°	100.2°
O4-P1-O5	120.1°	118.5°	117.2°	113.9°	113.9°	114.0°
O2-P6-O7	14.1°	12.6°	9.7°	16.2°	16.1°	12.3°
M12-O2-M10	100.7°	101.6°	106.5°	96.0°	97.7°	101.2°
O4-M12-O9	141.7°	140.2°	133.3°	146.3°	145.5°	137.1°
O5-M10-O8	142.9°	142.9°	136.7°	146.3°	145.1°	145.1°

	III_2Li_a	III_2Na_a	III_2K_a
P1-O3	1.639	1.670	1.693
P1-O2	1.608	1.587	1.576
P1-O4	1.532	1.538	1.536
P1-O5	1.541	1.538	1.536
O4-M7	1.835	2.176	2.510
O5-M8	1.841	2.176	2.510
O2-M7	1.871	2.214	2.581
O2-M8	1.861	2.214	2.581
O3-P1-O2	109.6°	102.2°	100.9°
O4-P1-O5	123.4°	119.3°	118.5°
M8-O2-M7	135.6°	150.8°	164.3°

Figure 7. Optimized structures at B3LYP/6-31+G(d) level of theory of the $[HPO_4\cdots Li_2\cdots PO_3]^-$ cluster (group **II**) and of the $[HPO_4\cdots Li_2]^-$ cluster (group **III**). Bond lengths are in angstroms and angles in degrees.

Discussion

In principle, the $[M^1M^2HP_2O_7]^-$ ions can be structurally characterized on the basis of CAD mass spectrometric results and energetic considerations resulting from our theoretical investigation.

The energy-resolved CAD mass spectra of $[M^1M^2HP_2O_7]^-$ ions ($M^1=M^2=Li^+$, Na^+, K^+) reported in Figure 2 show only one characteristic fragmentation corresponding to the loss of the $M^1M^2HPO_4$ molecule and leading to the PO_3^- fragment ion. The appearance energies of the PO_3^- fragment decrease with decreasing charge-to-radius ratio of the metal cation, in agreement with the calculated dissociation energies

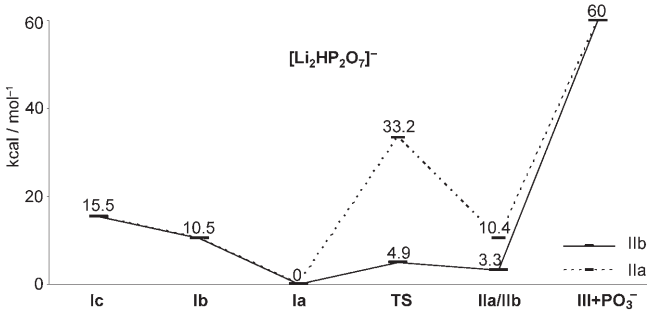

Figure 8. Schematic representation at the B3LYP/6-31+G(d) level of theory of the isomerization of the $Li_2HP_2O_7^-$ ions. All thermochemical parameters are in kcal mol^{-1} and were calculated at 298.15 K.

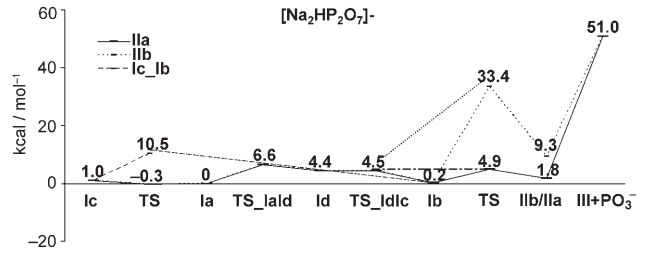

Figure 9. Schematic representation at B3LYP/6-31+G(d) level of theory of the isomerization of the $Na_2HP_2O_7^-$ ions. All thermochemical parameters are in kcal mol^{-1} and were calculated at 298.15 K.

the addition product ion **1**. Conversely, ions **3** are observed from $Na_2HP_2O_7^-$and $NaLiHP_2O_7^-$, but only in traces from $Li_2HP_2O_7^-$. The masses attributed to ionic products **1**, **2** and **3** are confirmed by the shift of two and four mass units, respectively, when $CH_3{}^{18}OH$ is introduced into the FT-ICR cell.

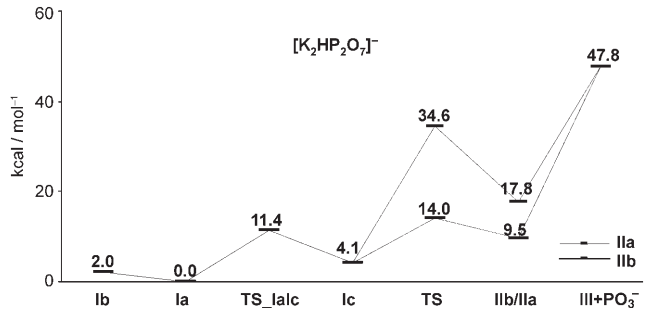

Figure 10. Schematic representation at B3LYP/6-31+G(d) level of theory of the isomerization of the $K_2HP_2O_7^-$ ions. All thermochemical parameters are in kcal mol^{-1} and are calculated at 298.15 K.

of cluster **II**. On the basis of quantum-mechanical calculations, this evidence is not structurally informative, because the PO_3^- ion can be formed directly by dissociation of cluster **II** or by a two-step process involving isomerization of ions **I** to **II**, whose barrier is considerably lower than the dissociation energy of cluster **II** (Figures 8–10). However, in conclusion, by considering the small stability differences and the low activation barriers of the **I**→**II** isomerizations, it seems reasonable to hypothesize the presence of both isomeric species **I** and **II** in the gaseous populations of $Li_2HP_2O_7^-$ and $Na_2HP_2O_7^-$.

The $K_2HP_2O_7^-$ potential energy surface reported in Figure 10 displays small but significant differences. Both the **I_2K_a**→**I_2K_c** and **I_2K_c**→**II_2K_a** isomerizations are characterized by higher energy barriers. Indeed, the **I_2K_a** ions are trapped in a relatively deep potential well and less able to isomerize to ions **II**. They probably represent the predominant species in the $K_2HP_2O_7^-$ ionic population.

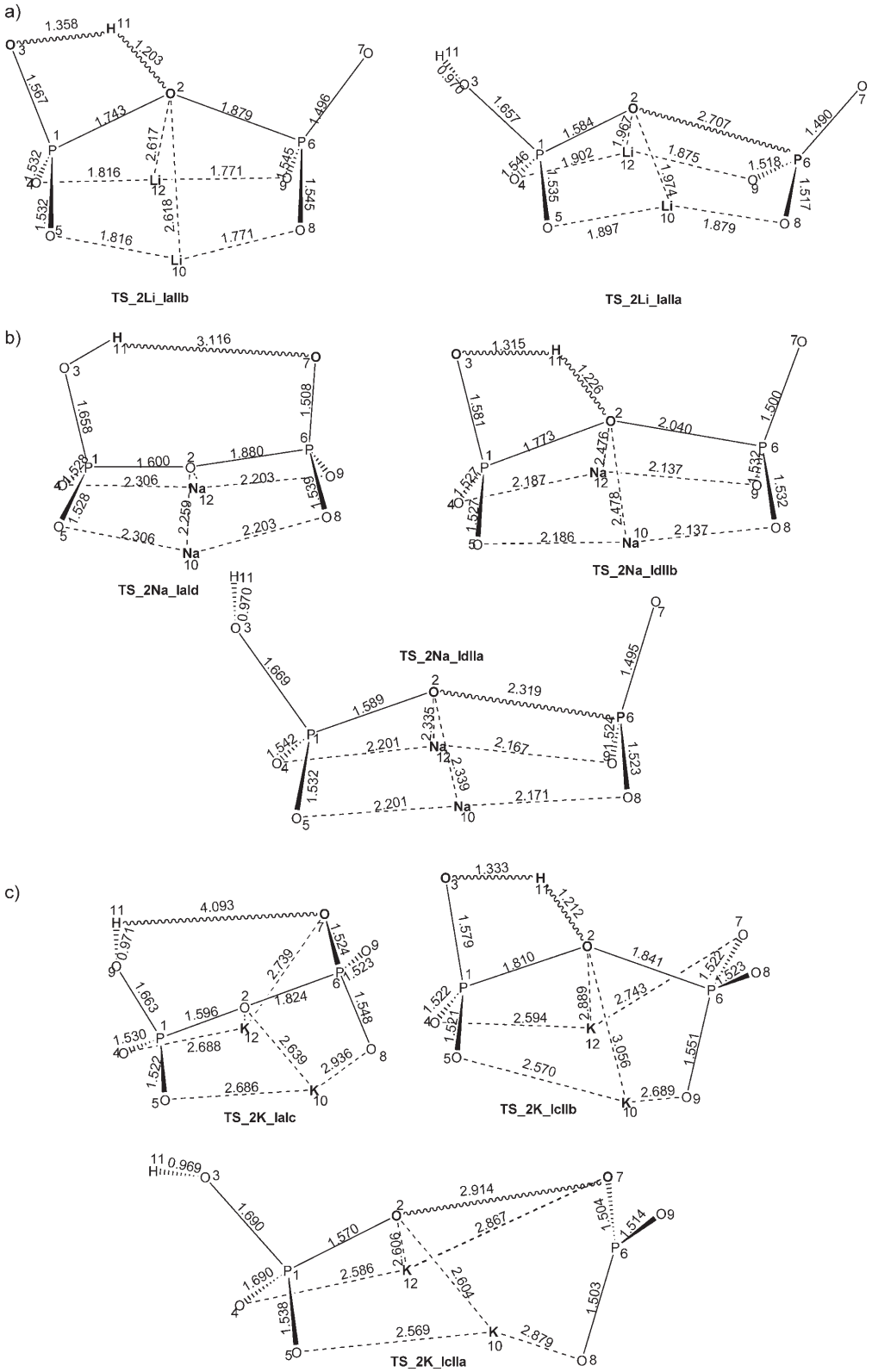

Figure 11. a) Transition-state geometries at the B3LYP/6-31+G(d) level of theory for the isomerization processes of the $Li_2HP_2O_7^-$ ions. b) Transition-state geometries at B3LYP/6-31+G(d) level of theory for the isomerization processes of the $Na_2HP_2O_7^-$ ions. c) Transition-state geometries at B3LYP/6-31+G(d) level of theory for the isomerization processes of the $K_2HP_2O_7^-$ ions.

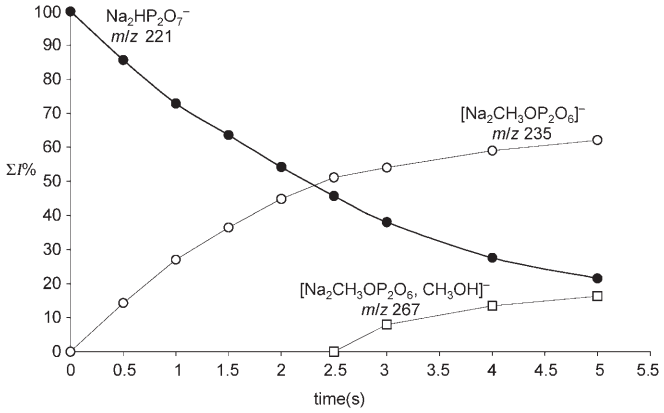

Figure 12. FT-ICR time profile of the ionic intensities of the reaction between $Na_2HP_2O_7^-$ ions and CH_3OH at a pressure of 1.8×10^{-8} mbar.

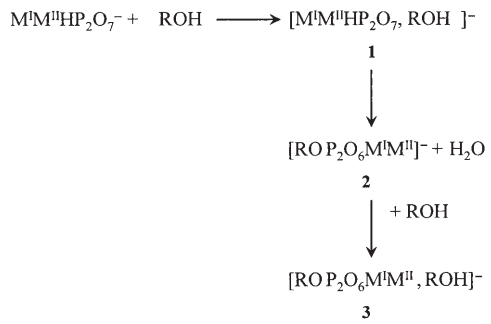

Scheme 1. Hypothesized mechanism for the reaction of gaseous $M_2HP_2O_7^-$ ions with alcohols.

Table 3. Rate constants for the reactions of $Na_2HP_2O_7^-$ ions with alcohols of different acidity, measured by FT-ICR/MS.

ROH	k_{exp} [10^{-9} mol cm^3 s^{-1}]	ΔH°_{acid}(ROH)[a] [kcal mol^{-1}]
CH_3OH	0.42	382.1
C_2H_5OH	0.67	378.0
CF_3CH_2OH	1.1	361.7
$(CF_3)_2CHOH$	1.1	345.0

[a] From ref. [45].

Table 4. Rate constants for the reactions of $M^1M^2HP_2O_7^-$ ions with CH_3OH, measured by FT-ICR/MS.

M^1,M^2	k_{exp} [10^{-9} mol cm^3 s^{-1}]
Li,Li	0.073
Na,Li	0.88
Na,Na	0.41
Na,K	0.070
K,K	–

The picture emerging from our systematic investigation of the gas-phase ion chemistry of diphosphate may allow generalized conclusions to be drawn which, when extended to the more complicated environmental conditions of enzymatic active sites, can facilitate a deep understanding of the mechanisms of enzymatic phosphate ester processes. Besides the specific interest in alkali metal coordination, the systematic investigation of species containing these cations is valuable in terms of mimicking the effects of noncovalent interactions between the phosphate group and metal cations or amino acid chains in enzymatic processes.

We devoted particular attention to the isomerization processes leading from diphosphate ions **I** to clusters **II**, since the reactions involving phosphate anions resulting in hydrolysis or transfer of the phosphoryl group can occur by a dissociative mechanism. Furthermore, the systematic investigation of the gas-phase reactivity of diphosphate species, hitherto unexplored, can provide information on the electronic requirements for phosphorus activation in phosphoryl-transfer reactions.

In agreement with previously reported results,[31] in our study[37] we found that the $H_3P_2O_7^-$ ion is a stable species in the gas phase, whose structure is characterized by the presence of two strong internal hydrogen bonds and by asymmetry of the P-O-P bonds. The $H_3P_2O_7^-$ ion is almost inert in the gas phase and, under the low-pressure conditions of FTICR mass spectrometry, able to undergo only reactions involving the phosphate oxygen atoms, such as proton transfer and clustering with strong acids. The most favored intramolecular isomerization to the $[H_3PO_4\cdots PO_3]^-$ cluster involves a proton shift to the bridging oxygen atom. This process is endothermic by 13.7 kcal mol^{-1} and has an activation barrier of 32.6 kcal mol^{-1} at the B3LYP/6-31+G(d) level of theory. The gas-phase dissociation energy of the $[H_3PO_4\cdots PO_3]^-$ cluster into H_3PO_4 and PO_3^- is 34.1 kcal mol^{-1}. In the $[MH_2P_2O_7]^-$ ions,[39] which correspond to the $H_2P_2O_7^{2-}$ ion coordinated with an alkali metal cation, the presence of a second negative charge increases the P-O-P angle and the P-O-P linkage is symmetric. An intramolecular proton shift to the bridging oxygen atom can lead to formation of the $[H_2PO_4\cdots M\cdots PO_3]^-$ cluster. This isomerization, the endothermicity of which does not change appreciably with respect to the $H_3P_2O_7^-$ ion for $M^+=Li$, becomes more favorable for $M^+=Na$ (5.3 kcal mol^{-1}). However, the $[H_2PO_4\cdots M\cdots PO_3]^-$ cluster has been characterized as an unstable species in the gas phase owing to its exothermic dissociation into MH_2PO_4 and PO_3^-. The $[MH_2P_2O_7]^-$ ions react by means of clustering reactions with acidic alcohols.

The $[M_2HP_2O_7]^-$ ions investigated in this work correspond to the $HP_2O_7^{3-}$ ion coordinated with two alkali metal cations. From the calculated orbital energies, it has been predicted that the $HP_2O_7^{3-}$ anion is a unstable species in the gas phase, but the presence of coordinated Mg^{2+} increases its stability.[33a] In the $HP_2O_7^{3-}$ structure,[31a,33a] elongation of one of the P–O bridging bonds to 1.706 Å and a P-O-P angle of 139.2° indicate the effect of electronic repulsion on inducing asymmetry in the bridging P–O bonds and larger P-O-P angles. A strong intramolecular H-bond between two phosphate groups characterizes the most stable $HP_2O_7^{3-}$ structure. Interestingly, the P-O-P angle increases to 156.9° and one P–O bridging bond is elongated to 1.764 Å in the structure in which this intramolecular interaction is absent.[31a] The reaction $HP_2O_7^{-3}\rightarrow HPO_4^{-2}+PO_3^-$ has been calculated to be strongly exothermic with a classical barrier height of 25.4 kcal mol^{-1} (HF).[31a]

In the $M_2HP_2O_7^-$ ions, the computed P-O-P angle is 128° for M = Li and 134.6° for M = Na, and the asymmetry of the P-O-P bond lengths increases with decreasing charge-to-radius ratio of the metal cation.

A different and more favorable isomerization process, namely, direct cleavage of the PO–P bond, can lead to formation of the $[HPO_4\cdots M^1,M^2\cdots PO_3]$ cluster. According to our computations, the process is endothermic by only 3.3 and 1.8 kcal mol^{-1} for $M^1 = M^2 = Li$ and $M^1 = M^2 = Na$, respectively. The barrier height relative to these isomerization processes of 4.9 kcal mol^{-1} for $M^1 = M^2 = Li$ and 0.5 kcal mol^{-1} $M^1 = M^2 = Na$ is significantly lower than the barrier for $HP_2O_7^{3-}$ dissociation. As is evident from the **TS_2Li_IaIIa** and the **TS_2Na_IdIIa** transition-state structures, the metal cations exert a catalytic effect by coordinating to the bridging oxygen atom, in agreement with the previously reported Mg–pyrophosphate isomerization energies.[33] In the $M_2HP_2O_7^-$ ions, the presence of three partially screened negative charges and the absence of the intramolecular hydrogen bond allows for larger P-O-P angles and bond lengths that facilitate direct breaking of the phosphate bridging linkage.

Among the roles suggested for a metal cation in accelerating dephosphorylation of polyphosphate, our results underline the importance of its relatively tight coordination to the transition state in the active enzymatic site.

Indeed, the **I_2Na_b** and **I_2Na_d** structures are characterized by oxygen atoms in staggered or eclipsed conformations, respectively, and by the lack of an H-bond. As shown in Figure 9, on breaking of the H-bond the **I_2Na_a** ion can yield the **I_2Na_b** ion, in which electrostatic repulsions are partially offset by staggering the oxygen atoms. The easy isomerization of this ion to the **I_2Na_d** ion, obtained by rotation around the P-O-P bond, allows the oxygen atoms of the diphosphate ion to go back into the eclipsed configuration. As a consequence, the P1–O2 bond lengthens to 1.954 Å, the P-O-P angle increases up to 150° and cleavage of a P–O bond can occur. During enzymatic processes, it seems likely that relatively tight coordination of the oxygen atoms with amino acid residues or metal cations prevents P-O-P rotation, allows the eclipsed conformation to be maintained and facilitates P-O-P bond breaking.

With respect to the diphosphate species previously investigated, the gaseous $[M^1M^2HP_2O_7]^-$ ions are sufficiently activated to react with acidic alcohols with elimination of a water molecule.

The main features of the reaction of $[M^1M^2HP_2O_7]^-$ ions with alcohols in the gas phase can be summarized as follows:

1) The acidity difference between the alcohol molecule and the phosphate anion strongly influences the overall reaction efficiency. The reaction proceeds at unit efficiency with acidic alcohols such as $(CF_3)_2CHOH$, which suggests the importance of an H-bond in a concerted mechanism, or of proton transfer in the rate-determining step of the reaction.
2) The rate constants measured for reaction of the $[M^1M^2HP_2O_7]^-$ ions with methanol highlight the role played by the alkali metal cation in the rate-determining step. Note that the more basic $Na_2HP_2O_7^-$ reacts more slowly than the less basic $NaLiHP_2O_7^-$. Finally $K_2HP_2O_7^-$ ions do not react with methanol.

The most reasonable hypothesis to account for the increased reactivity of these phosphate species is based on their higher basicity. The gas-phase proton affinities were evaluated by ab initio quantum-mechanical methods[31b] as 323 kcal mol^{-1} for the $H_3P_2O_7^-$ monoanion, 416 kcal mol^{-1} for the $H_2P_2O_7^{2-}$ dianion and 544 kcal mol^{-1} for the $HP_2O_7^{3-}$ trianion. Replacing one hydrogen atom of $H_3P_2O_7^-$ by Li or Na gives a proton affinity of 328 kcal mol^{-1} for the $LiH_2P_2O_7^-$ ion and 336 kcal mol^{-1} for the $NaH_2P_2O_7^-$ ion.[31b] Replacement of the second H atom by Li or Na should have a similar effect. Indeed, since direct evaluation of the gas-phase proton affinities of the $M_2HP_2O_7^-$ ions has never been reported, an upper limit of 400 kcal mol^{-1} can be safely estimated. Proton transfer from all the alcohols used would probably be energetically favored.

As far as the mechanism of the gas-phase $[M_2HP_2O_7]^-$ reaction with acidic alcohols is concerned, there are two main open questions regarding the nature of the reacting phosphate ion and the role played by the ROH molecule. Both are related to the more general question of the mechanism of phosphoryl-transfer reactions. To the best of our knowledge, no kinetic or thermodynamic experimental data for the gas-phase reaction of inorganic polyphosphate anions with alcohols have been reported till now. Recent ab initio calculations on the thiolysis and alcoholysis of phosphate tri- and monoesters with alkyl and aryl leaving groups[36] indicate that the reaction of triesters proceeds through an associative pathway, but monoester phosphates can react by both associative and dissociative mechanisms, depending on the basicity of the attacking and leaving groups. All the reactions of monoesters involve two intramolecular H^+ transfers: from the nucleophile to the phosphate group and from the phosphate to the leaving group. According to the associative mechanism ($A_n + D_n$), in the ion–molecule complex formed by the alcohol and the monoester monoanion, the alcohol or thiol hydrogen atom is coordinated to one of the ionized phosphate oxygen atoms, while the oxygen or sulfur atom of the nucleophile coordinates to phosphorus. The associative intermediates have trigonal-bipyramidal (tbp) geometries with the nucleophile and leaving group in the axial positions and the phosphate group oxygen atoms (protonated and nonbonding) in the equatorial positions. For the reaction of $CH_3OPO_3H^-$ with methanol the calculated energy barriers relative to nucleophilic attack of CH_3OH at the phosphorus atom and CH_3OH departure from the tpb intermediate are around 20 kcal mol^{-1}. According to the dissociative mechanism ($D_n + A_n$), following intramolecular dissociation of $CH_3OPO_3H^-$ promoted by H^+ shift to the bridging oxygen atom, the nucleophile CH_3OH attacks the metaphosphate ion. The computed energy barriers involved in these

steps are about 10 kcal mol^{-1} higher than those of the associative mechanism.

In the light of these results, the mechanistic hypothesis for the reaction of phosphate monoesters and alcohols can be extended to the reaction of the $M_2HP_2O_7^-$ ions. However, the main difference is the higher basicity of these ions, which should prove capable of deprotonating the alcohol molecule. According to the associative pathway, the alcohol molecule or, if formed, the alkoxide ion, could attack the phosphorus atom, and the phosphorane intermediate should subsequently eliminate the water molecule. The dissociative pathway should proceed through the isomerization of ions **I** to **II**, and the reaction of the HPO_4^{2-} moiety with the alcohol is followed by elimination of a water molecule.

Metal cations that partially screen the negative charge of the phosphate anion should favor phosphate protonation, whereas the electrophilic character of the phosphorus atom should be increased by the presence of alkali metal cations having high charge-to-radius ratio, such as Li^+. On the basis of these considerations, it seems possible to justify the higher reactivity of the $LiNaHP_2O_7^-$ ion with respect to the $Li_2HP_2O_7^-$ and $Na_2HP_2O_7^-$ ions and the inability of the $K_2HP_2O_7^-$ ions to react with alcohols, since these species are not sufficiently activated to undergo nucleophilic attack at the phosphorus atom. However, the chemical inertness of the $K_2HP_2O_7^-$ ions could find a second possible explanation in the lack of group **II** ions in the $K_2HP_2O_7^-$ ionic population.

Finally, a third mechanistic alternative could be hypothesized. The alkoxide ion formed by proton transfer from the alcohol to the $M_2HP_2O_7^-$ ions remains trapped by the metal cation and acts as a spectator of water molecule elimination from protonated ions **I** or **II**.

The experimental information reported in this work cannot draw definitive conclusions on the gas-phase mechanism of the reaction between the $M_2HP_2O_7^-$ ions and alcohols. Theoretical and experimental efforts are underway to probe the mechanism of this reaction by using labeled $H_2{}^{18}O$.

Conclusion

The gas-phase ion chemistry of inorganic polyphosphate species is still largely unexplored, yet it could contribute to clarifying the factors affecting the stability and reactivity of these species in their enzymatic processes. In this context, the results presented here represent an important addition to our systematic investigation of the gas-phase properties of inorganic phosphate. The coordination of $HP_2O_7^{3-}$ ions with two M^+ ions allows experimental observation of $M_2HP_2O_7^-$ ions. However, the electrostatic repulsions between the partially screened negative charges facilitate isomerization of the gaseous $[M^1M^2HP_2O_7]^-$ ions ($M^1=M^2$ or $M^1\neq M^2$ and M^1,M^2=Li^+, Na^+, K^+, Rb^+, Cs^+) in which a linear diphosphate anion is coordinated to two M^+ ions (group **I**) to the $[PO_3\cdots M^1,M^2\cdots HPO_4]^-$ clusters (group **II**). The relative gas-phase stabilities of these species and the activation barriers for the **I**→**II** isomerization, which depend on the nature of the M^+ cations, together with the high dissociation energies of cluster **II**, allow the existence of both these species to be hypothesized in the gaseous ionic population of $M_2HP_2O_7^-$ ions. The previously unexplored gas-phase reactivity of $[M^1M^2HP_2O_7]^-$ ions towards alcohols of different acidity was investigated by FT-ICR/MS. The reaction proceeds through the addition of the alcohol molecule followed by elimination of a water molecule.

Experimental Section

Materials: $Na_4P_2O_7\cdot 10H_2O$, $K_4P_2O_7$, $Na_5P_3O_{10}$, MOH, MNO_3 (M = Li, Na K, Cs, Rb) and all other chemicals were purchased from Sigma-Aldrich Ltd. and used as received.

Mass spectrometric experiments: ESI-FTICR/MS experiments were performed with a Bruker BioApex 4.7 T FT-ICR mass spectrometer equipped with an Analytica of Brandford Electrospray Ionization Source. Samples were infused into a fused-silica capillary (i.d. 50 μm) at a flow rate of 130 μL h^{-1}, and the ions accumulated in a hexapole ion guide for 0.8 s. Typical ESI voltages for cylinder, capillary and end plates were 3000, 4000 and 4300 V respectively. The capillary exit and skimmer voltages were set to about −60 and −10 V, respectively and hexapole d.c. offset was set to 0.7 V.

Triple-quadrupole (TQ) mass spectra were recorded on a TSQ 700 mass spectrometer from Finnigan Ltd. operating in the negative-ion mode. The $M_2HP_2O_7^-$ ions were obtained in the ESI source of the FT-ICR and TQ mass spectrometers by electrospray ionization of acetonitrile/water (1/1) solutions of $Na_5P_3O_{10}$ and a source of M^+ cations (M salts or MOH), $Na_4P_2O_7$ or $K_4P_2O_7$. ESI solutions were prepared daily at a concentration of 10^{-4} M and used immediately for analysis. In the FT-ICR experiments, the $M_2HP_2O_7^-$ ions were transferred to the resonance cell (25 °C) and isolated by broad-band and "single-shot" ejection pulses. After thermalization with Ar introduced into the cell through a pulsed valve, the ions were re-isolated by "single shots" and allowed to react with reagents in the cell. The pressure of the neutral reactants ranged from 10^{-8} to 10^{-7} mbar and was measured by a Bayard–Alpert ionization gauge, whose readings were calibrated using, as a reference, the known rate coefficient of the $CH_4+CH_4^+\rightarrow CH_5^++CH_3^{\cdot}$ reaction. The readings were corrected for the relative sensitivity to the various gases used according to a standard method.[40] The pseudo-first-order rate constants were obtained by plotting $\lg(I_t/I_{t=0})$ of $[M_2HP_2O_7]^-$ as a function of reaction time. Then the bimolecular rate constants were determined from the number density of the neutral molecules, deduced in turn from the pressure of the gas. Average dipole orientation (ADO) collision rate constants k_{ADO} were calculated as described by Su and Bowers.[41] Reaction efficiencies (RE) are the ratio of the experimental rate constants k_{exp} to the collision rate constants k_{ADO}. The absolute uncertainty of each rate constant was estimated to be 30%.

In the TQ mass spectrometric experiments, the $M_2HP_2O_7^-$ ions generated in the ESI source were isolated by the first quadrupole (Q1) and driven into the collision cell, actually an RF-only hexapole, containing the neutral reagent at a pressure of up to 1 mTorr. Collisionally activated dissociation (CAD) experiments were performed by utilizing Ar as target gas at a pressure of $(1–5)\times10^{-4}$ Torr and at a collision energy ranging from 0 to 50 eV (laboratory frame). Laboratory (lab) ion energies are converted to energies in the centre-of-mass frame (cm) by using the formula $E_{cm}=E_{lab}m/(m+M)$ where m and M are the neutral Ar and ionic reactants, respectively. The charged products were analyzed with the third quadrupole, scanned at a frequency of 150 amu s^{-1}.

Computational details: All calculations were carried out using the Gaussian 03 package.[42] All structures were fully optimized and characterized as minima or transition states by calculating the harmonic vibrational fre-

quencies at the B3LYP/6-31+G(d) level.[43] At these geometries single-point energy evaluations were done at B3LYP/6-311+G(2df,2dp), MP2/6–311+G(2df,2dp)[43] and CCSD(T)/6-31+G(d) levels.[43] Zero-point energies (ZPE), thermal contributions to thermodynamic functions and activation parameters were computed from B3LYP/6-31+G(d) structures, and harmonic frequencies by using the rigid rotor/harmonic oscillator approximation and the standard expressions for an ideal gas in the canonical ensemble at 298.15 K and 1 atm.

Acknowledgements

Financial Support from the Italian Ministero dell'Università e della Ricerca Scientifica e Tecnologica (MURST) is gratefully acknowledged. The authors thank the Campus Grid of the University of Naples for computer facilities.

[1] F. H. Westheimer, *Science* **1987**, *235*, 1173.
[2] R. Wolfeden, M. J. Snider, *Acc. Chem. Res.* **2001**, *34*, 938, and references therein.
[3] A. G. Cassano, V. E. Andreson, M. E. Harris, *Biochemistry* **2004**, *43*, 10547.
[4] K. Kirby, M. F. Lima, D. da Silva, F. Nome, *J. Am. Chem. Soc.* **2004**, *126*, 1350, and references therein.
[5] G. P. K. Grzyska, P. G. Czyryca, J. Purcell, A. C. Hengge, *J. Am. Chem. Soc.* **2003**, *125*, 43, 13106, and references therein.
[6] H.-H. de Jager, A. M. Heyns, *J. Phys. Chem. A* **1998**, *102*, 2838.
[7] J. Aqvist, K. Kolmodin, J. Florian, A. Warshell, *Chem. Biol.* **1999**, *6*, R71.
[8] J. Purcell, A. C. Hengge, *J. Org. Chem.* **2005**, *70*, 8437.
[9] a) J. Florian, J. Aqvist, A. Warshel, *J. Am. Chem. Soc.* 1998, 120, 11524; b) J. Florian, J. Aqvist, A. Warshel, *J. Am. Chem. Soc.* **1997**, *119*, 5473.
[10] P. Imhof, S. Fisher, R. Kramer, J. C. Smith, *THEOCHEM* **2005**, *713*, 1.
[11] Y.-Ni. Wang, I. A. Topol, J. R. Collins, S. K. Burt, *J. Am. Chem. Soc.* **2003**, *125*, 13265, and references therein.
[12] J. Akola, R. O. Jones, *J. Am. Chem. Soc.* **2003**, *125*, 5473, and references therein.
[13] R. A. Torres, F. Himo, T. C. Bruice, L. Noodleman, T. Lovell, *J. Am. Chem. Soc.* **2003**, *125*, 9861.
[14] X. Lopez, M. Schaefer, A. Dejaegere, M. Karplus, *J. Am. Chem. Soc.* **2002**, *124*, 5010, and references therein.
[15] C.-H. Hu, T. Brinck, *J. Phys. Chem. A* **1999**, *103*, 5379, and references therein.
[16] D. E. Wilcox, *Chem. Rev.* **1996**, *96*, 2435.
[17] a) J. Florian, A. Warshel, *J. Phys. Chem. B* **1998**, *102*, 719, and references therein; b) M. Fothergill, M. F. Goodman, J. Petruska, A. Warshel, *J. Am. Chem. Soc.* **1995**, *117*, 11620.
[18] a) J. Aqvist, A. Warhel, *J. Am. Chem. Soc.* **1990**, *112*, 2860; b) J. Floriàn, M. F. Goodman, A. Warshel, *J. Am. Chem. Soc.* **2003**, *125*, 8163.
[19] E. A. Galburt, B. L. Stoddard, *Biochemistry* **2002**, *41*, 13851.
[20] a) P. Molenveld, J. F. J. Engbersen, D. Reinhoudt, *Chem. Soc. Rev.* **2000**, *29*, 75; b) M. Padovani, N. H. Williams, P. Wyman, *J. Phys. Org. Chem.* **2004**, *17*, 472.
[21] C. Vichard, T. A. Kaden, *Inorg. Chim. Acta* **2004**, *357*, 2285.
[22] T. Humphry, M. Forconi, N. H. Williams, A. C. Hengge, *J. Am. Chem. Soc.* **2004**, *126*, 11864.
[23] a) T. Blades, Y. Ho, P. J. Kebarle, *J. Am. Chem. Soc.* **1996**, *118*, 196, and references therein b) A. T. Blades, Y. Ho, P. J. Kebarle, *J. Phys. Chem.* **1996**, *100*, 2443.
[24] X.-B. Wang, E. R. Vorpagel, X. Yang, L.-S. Wang, *J. Phys. Chem. A* **2001**, *105*, 10468.
[25] B. K. Choi, D. M. Hercules, M. Houalla, *Anal. Chem.* **2000**, *72*, 5087.
[26] R. R. Julian, J. L. Beauchamp, *Int. J. Mass Spectrom.* **2003**, *227*, 147.
[27] S. Gronert, R. A. J. O'Hair, *J. Am. Soc. Mass Spectrom.* **2002**, *13*, 1088.
[28] R. M. Burke, J. K. Pearce, W. E. Boxford, A. Brukmann, C. E. H. Dessent, *J. Phys. Chem. A* **2005**, *109*, 9775.
[29] H. A. Cox, R. Hodyss, J. L. Beauchamp, *J. Am. Chem. Soc.* **2005**, *127*, 4084.
[30] a) H. Saint-Martin, I. Ortega-Blake, A. Les, L. Adamowicz, *Biochim. Biophys. Acta* **1991**, *1080*, 205; b) E. Colvin, E. Evleth, Y. Akacem, *J. Am. Chem. Soc.* **1995**, *117*, 4357; c) H. Saint-Martin, I. Ortega-Blake, A. Les, L. Adamowicz, *Biochim. Biophys. Acta* **1994**, *1207*, 12.
[31] a) B. Ma, C. Meredith, H. F. Schaefer, *J. Phys. Chem.* **1995**, *99*, 3815; b) B. Ma, C. Meredith, H. F. Schaefer, *J. Phys. Chem.* **1994**, *98*, 8216, and references therein.
[32] W. J. McCarthy, L. Adamowicz, H. Saint-Martin, I. Ortega-Blake, *Revista de la Soc. Quimica de Mexico* **2002**, *46*, 145.
[33] a) H. Saint-Martin, L. E. Ruiz-Vicent, A. Ramirez-Solìs, I. Ortega-Blake, *J. Am. Chem. Soc.* **1996**, *118*, 12167; b) W. J. McCarthy, D. M. Smith, L. Adamowicz, H. Saint-Martin, I. Ortega-Blake, *J. Am. Chem. Soc.* **1998**, *120*, 6113; c) H. Saint-Martin, L. E. Vicent, *J. Phys. Chem. A* **1999**, *103*, 6862.
[34] a) R. V. S. Hodges, A. Sullivan, J. L. Beauchamp, *J. Am. Chem. Soc.* **1980**, *102*, 937, 20; b) R. C. Lum, J. J. Grabowski, *J. Am. Chem. Soc.* **1992**, *114*, 8619; c) R. C. Lum, J. J. Grabowski, *J. Am. Chem. Soc.* **1993**, *115*, 7823.
[35] J.-F. Gal, M. Herreros, P. C. Maria, L. Operti, C. Pettigiani, R. Rabezzana, G. A. Vaglio, *J. Mass Spectrom.* **1999**, *34*, 1296.
[36] G. M. Arantes, H. Chaimovich, *J. Phys. Chem. A* **2005**, *109*, 5625, and references therein.
[37] F. Pepi, A. Ricci, M. Rosi, M. Di Stefano, *Chem. Eur. J.* **2004**, *10*, 840.
[38] F. Pepi, A. Ricci, M. Rosi, M. Di Stefano, *Chem. Eur. J.* **2004**, *10*, 5706.
[39] F. Pepi, A. Ricci, M. Rosi, M. Di Stefano, *Chem. Eur. J.* **2006**, *12*, 2787.
[40] J. E. Bartmess, R. M. Georgiadis, *Vacuum* **1983**, *33*, 149.
[41] T. Su, M. T. Bowers, *Int. J. Mass Spectrom. Ion Phys.* **1973**, *12*, 347.
[42] Gaussian 03 (Revision C.02), M. J. Frisch, G. W. Trucks, H. B. Schlegel, G. E. Scuseria, M. A. Robb, J. R. Cheeseman, J. A. Montgomery, Jr., T. Vreven, K. N. Kudin, J. C. Burant, J. M. Millam, S. S. Iyengar, J. Tomasi, V. Barone, B. Mennucci, M. Cossi, G. Scalmani, N. Rega, G. A. Petersson, H. Nakatsuji, M. Hada, M. Ehara, K. Toyota, R. Fukuda, J. Hasegawa, M. Ishida, T. Nakajima, Y. Honda, O. Kitao, H. Nakai, M. Klene, X. Li, J. E. Knox, H. P. Hratchian, J. B. Cross, V. Bakken, C. Adamo, J. Jaramillo, R. Gomperts, R. E. Stratmann, O. Yazyev, A. J. Austin, R. Cammi, C. Pomelli, J. W. Ochterski, P. Y. Ayala, K. Morokuma, G. A. Voth, P. Salvador, J. J. Dannenberg, V. G. Zakrzewski, S. Dapprich, A. D. Daniels, M. C. Strain, O. Farkas, D. K. Malick, A. D. Rabuck, K. Raghavachari, J. B. Foresman, J. V. Ortiz, Q. Cui, A. G. Baboul, S. Clifford, J. Cioslowski, B. B. Stefanov, G. Liu, A. Liashenko, P. Piskorz, I. Komaromi, R. L. Martin, D. J. Fox, T. Keith, M. A. Al-Laham, C. Y. Peng, A. Nanayakkara, M. Challacombe, P. M. W. Gill, B. Johnson, W. Chen, M. W. Wong, C. Gonzalez, J. A. Pople, Gaussian, Inc., Wallingford CT, **2004**.
[43] A description of basis sets and standard computational methods can be found in J. B. Foresman, A. E. Frisch, *Exploring Chemistry with Electronic Structure Methods*, 2nd ed., Gaussian Inc., Pittsburg, PA, **1996**.
[44] V. Barone, *J. Chem. Phys.* **2004**, *120*, 3059.
[45] NIST Chemistry WebBook: NIST standard Reference Database No. 69, February **2000** release; data collection of the National Institute of Standards and Technology. Available from http://webbook.nist.gov.

Received: July 27, 2006
Published online: December 4, 2006

